Thermally Cross-Linkable Hole-Transporting Materials for Improving Hole Injection in Multilayer Blue-Emitting Phosphorescent Polymer Light-Emitting Diodes

Michelle S. Liu, Yu-Hua Niu, Jae-Won Ka, Hin-Lap Yip, Fei Huang, Jingdong Luo, Tae-Dong Kim, and Alex K.-Y. Jen*

Department of Materials Science & Engineering, University of Washington, Box 352120, Seattle, Washington 98195-2120

Received June 18, 2008; Revised Manuscript Received November 3, 2008

ABSTRACT: One of the most challenging tasks in fabricating multilayer polymer light-emitting diodes (PLEDs) is to develop robust hole-transporting materials that possess matched energy level with indium tin oxide (ITO) anode and the highest occupied molecular orbital (HOMO) of light-emitting polymers to facilitate efficient hole injection and transport. In this article, a series of thermally cross-linkable 4,4′,4″-tris(*N*-carbazolyl)triphenylamine (TCTA) derivatives have been synthesized to explore their function as efficient hole-transporting materials for blue-emitting electrophorphorescent devices. In particular, their excellent solvent resistance enables them to be used in the double hole-transporting layer (HTL) device configuration to facilitate cascade hole injection. The effects of cross-linking temperature and the functional group on the compatibility between two HTLs are investigated through optical and atomic force microscopy. When vinylbenzyl ether is used as the cross-linking group for TCTA, it shows the best compatibility with the bottom HTL. The resulting blue light-emitting device reaches a peak external quantum efficiency of 3.17%, corresponding to a current efficiency of 6.6 cd/A. These values are much higher than those of the PLEDs using conventional PEDOT/PSS as a single HTL. The improvements in the device performance are due to reduced hole-injection barrier and better electron/exciton confinement.

Introduction

Hole-transporting layer (HTL) plays a very important role in fabricating high efficiency multilayer polymer light-emitting diodes (PLEDs).[1] It enhances hole injection from indium tin oxide (ITO) anode into light-emitting layer (EML), which results in balanced charge-injection/transport and better device performance. To be used as an efficient HTL in multilayer PLEDs, the material needs to possess very good solvent resistance for multilayer processing. To achieve this, the commonly employed approaches use either a photo- or thermally cross-linked hole-transporting material or a suitable solvent combination to avoid dissolution of the bottom layer.[2−10]

Recently, the efficiency of PLEDs has been significantly increased by the incorporation of phosphorescent dopants in polymer hosts to harvest both singlet and triplet excitons.[11−15] In this case, in addition to directly charge trapping to form emissive excitons on the dopants, both singlet and triplet excitons formed in the host can also be transferred to dopants via the Föster and Dexter energy transfer processes, allowing the device to reach very high efficiency. In blue- or green-emitting electrophosphorescent PLEDs, which involve the use of high-energy phosphors, large bandgap host materials with triplet energy higher than that of the phosphorescent emitter are needed to avoid back energy transfer from the triplet dopants to the host/exciton.[16,17] Because of the high HOMO (highest occupied molecular orbital) energy level of these large gap hosts (usually greater than −5.8 eV), it is difficult to achieve efficient hole injection from ITO to the EML if only a single HTL is employed in the device. Therefore, multiple HTLs with stepped energy profiles are necessary for achieving efficient hole injection and charge confinement.

For small-molecule-based organic light-emitting diodes (OLEDs), this could be easily achieved through vacuum deposition;[18−20] however, realizing such a multi-HTL structure in PLEDs is quite challenging. In addition to the need of having good solvent resistance, obtaining good compatibility between HTLs is also very important for ensuring good contact at the interface. Recently, cascade hole injection has been demonstrated through layer-by-layer deposition of photo-cross-linkable triarylamine derivatives with oxetane functionality.[21] In addition, several other polymers such as poly(*p*-phenylenevinylene) (PPV), poly(*N*-vinylcarbazole) (PVK), poly(2,7-(9,9-di-*n*-octylfluorene)-*alt*-(1,4-phenylene-((4-*sec*-butyl phenyl)imino)-1,4-phenylene) (TFB), and an ethanol-soluble PVK salt, PVK-SO_3Li, have also been mentioned as suitable materials for functioning as the second HTL between poly(3,4-ethylenedioxythiophene)/(polystyrene sulfonate) (PEDOT/PSS) and EML.[22−26] However, there are several drawbacks associated with these polymer HTLs. For example, PVK and TFB can still be dissolved in the solvents used for spin coating the upper EML. This prevents their wide use as HTL in the solution-processed PLEDs. In other cases, the reactive byproducts produced during the conversion process of PPV and the metal ions associated with the PVK-SO_3Li backbone are detrimental to the long-term stability of devices. In addition to these problems, none of above-mentioned materials possess high enough triplet energy to confine the high-energy blue-emitting excitons within the EML, which further limits their use in the electrophosphorescent devices.[27]

In our earlier work, we demonstrated the successful development of a highly efficient, thermally cross-linkable hole-injecting/-transporting polystyrene derivative (PS-TPD-PFCB) that possesses the pendent TPD as side chains for hole transporting and phenyl trifluorovinyl ether (TFV) as the cross-linker (Figure 1).[28] Bilayer fluorescent PLEDs using this polymer as the HTL have shown higher quantum efficiency and brightness than the devices using conventional PEDOT/PSS as HTL. However, its HOMO energy level (−5.3 eV) is rather low; therefore, there is still a significant energy barrier for

* Corresponding author. E-mail: ajen@u.washington.edu.

10.1021/ma801374w CCC: $40.75
Published on Web 11/26/2008

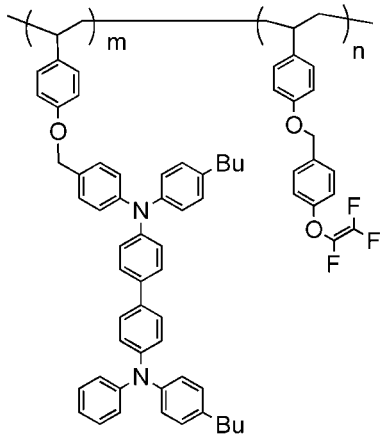

PS-TPD-TFV

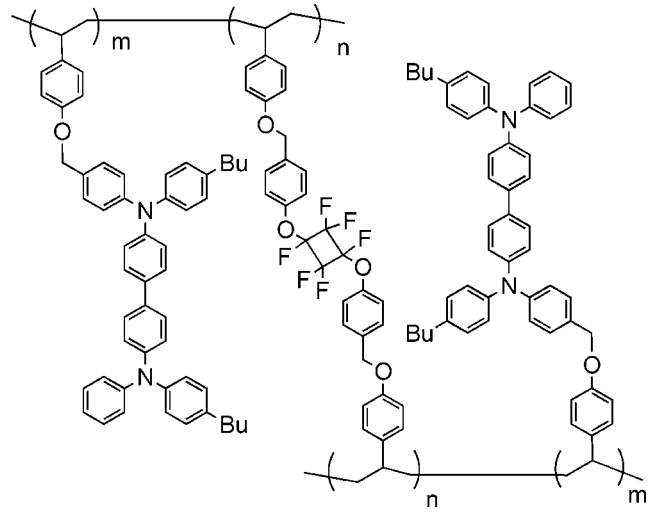

PS-TPD-PFCB

Figure 1. Chemical structures of PS-TPD-TFV and PS-TPD-PFCB.

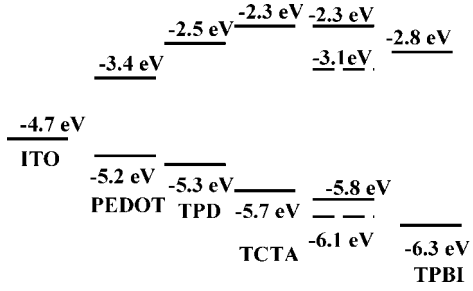

Figure 2. Energy diagram of PLED components. The energy levels of TPD, TCTA, PEDOT/PSS, PVK, FIr6, and TPBI are cited from the literature.

injecting holes into the EML in the blue-emitting phosphorescent devices if PS-TPD-PFCB is used as single HTL. To solve this problem, we have developed a new family of thermally cross-linkable 4,4′,4″-tris(*N*-carbazolyl)triphenylamine (TCTA) derivatives that bear either TFV or vinylbenzyl ether (VB) cross-linking groups. These TCTA derivatives can be applied as a robust second HTL between PS-TPD-PFCB and the EML. Because TCTA possesses a higher HOMO energy level (−5.7 eV)[18] than TPDs (−5.3 eV) (Figure 2), these cross-linkable TCTA derivatives allow us to create a gradient energy pathway for injecting holes into blue-emitting electrophosphorescent devices. When TFV and VB groups react, they do not require any chemical initiators nor do they produce any byproducts, which are very beneficial to the device durability. A nonconjugated polymer, PVK, was used as the host, and the blue phosphor, iridium(III)*bis*(4′,6′-difluorophenylpyridinato)tetrakis(1-pyrazolyl) borate (FIr6), was used as the dopant emitter in this study.[29] Although PVK and FIr6 have high HOMO energies of −5.8[30] and −6.1 eV, respectively, it is still possible to inject holes efficiently from ITO through TPD and TCTA into this EML. Moreover, the TCTA-containing HTLs provide better electron and exciton confinement through their higher LUMO energy level (−2.3 vs −2.5 eV)[31] and larger bandgap (3.4 vs 2.8 eV) compared with the TPD-containing hole-transporting materials.[32] To apply this favorable energetic to build efficient blue phosphorescent PLEDs, the effects of different cross-linkable functional groups and reaction conditions on the morphology and compatibility of TCTA derivatives and PS-TPD-PFCB were systematically investigated.

Experimental Section

Materials and Methods. All chemicals were purchased from Aldrich and were used as received unless otherwise specified. Tetrahydrofuran (THF) and ether were distilled under nitrogen from sodium with benzophenone as the indicator. FIr6 and 1,3,5-tris(*N*-phenyl bezimidazol-2-yl)benzene (TPBI) were synthesized following the literature procedures.[33,34] ^{1}H NMR spectra were taken on a Bruker AV-300 (300 MHz) spectrometer with tetramethylsilane (TMS) as the internal reference. ^{13}C NMR spectra were taken on a Bruker AV-500 (500 MHz) spectrometer. ESI-MS spectra were recorded on a Bruker Daltonics Esquire liquid chromatograph−ion trap mass spectrometer. Elemental analysis was determined at Midwest Microlabs. Cyclic voltametric data were measured on a BAS CV-50W voltametric analyzer. Cyclic voltammograms of the TCTA derivatives (0.5 mM) in a 0.1 M electrolyte solution of tetrabutylammonium hexafluorophosphate in dichloroethane (DCE) were obtained at 100 mV/s sweep rate with platinum as both the working and auxiliary electrodes and Ag^+/Ag as the reference electrode. Thermal transitions were measured by TA Instruments thermogravimetric analysis (TGA) 2950 and differential scanning calorimetry (DSC) 2010 under a nitrogen atmosphere at a heating rate of 10 °C/min. UV−vis absorption spectra were measured using a Perkin-Elmer Lambda 9 UV/vis/NIR spectrophotometer. A Digital Instruments Nanoscope III atomic force microscope installed with etched silicon tips with a typical resonant frequency of 300−350 kHz and an Olympus BX 60 optical microscope were used to probe the film morphology of TCTA derivatives.

Tris(4-iodophenyl)amine (1). To a stirred mixture of triphenylamine (7.36 g, 30.0 mmol) and *N*-iodosuccinimide (NIS, 21.60 g, 96.0 mmol) in chloroform (180 mL) was added acetic acid (120 mL) at room temperature under the exclusion of light. The solution was stirred overnight at room temperature. The reaction mixture was poured in water, washed with sodium thiosulfate, and extracted with methylene chloride. The combined methylene chloride layers were washed with water, dried with Na_2SO_4, and concentrated. The crude product was purified over a silica gel column with hexane/methylene chloride (7:1) as eluent to afford a slightly brown solid (16.54 g, 88%). ^{1}H (300 MHz, $CDCl_3$, δ): 7.56 (d, 6H, J = 8.7 Hz), 6.83 (d, 6H, J = 9.0 Hz).

4, 4′,4″-Tris(*N*-carbazolyl)triphenylamine (TCTA, 2). To a stirred mixture of tris(4-iodophenyl)amine (9.34 g, 15.0 mmol), carbazole (10.03 g, 60.0 mmol), copper powder (750 mg, 11.8 mmol), and potassium carbonate (16.2 g, 117.2 mmol) was added nitrobenzene (40 mL) under nitrogen. The mixture was refluxed for 3 days. The hot solution was filtered, and the filtrate was added

dropwise in methanol. The precipitate was then filtered and washed with methanol and water successively. It was then redissolved in benzene and purified through a silica gel column with a gradient solvent of hexane to hexane/toluene (3:2) as eluent to afford a slightly brown solid (7.88 g, 71%). ^{1}H (300 MHz, $CDCl_3$, δ): 8.17 (d, 6H, J = 8.1 Hz), 7.60−7.42 (m, 24H), 7.31 (t, 6H, J = 7.5 Hz). ^{13}C NMR (125 MHz, $CDCl_3$, δ): 150.47, 145.04, 136.89, 132.38, 130.04, 129.43, 127.43, 124.45, 124.04, 113.89.

TCTA-3CHO (3). To stirred *N*′*N*-dimethylformamide (DMF) (10.97 g, 150 mmol) was added dropwise $POCl_3$ (3.78 g, 25 mmol) at 0 °C; the resulting solution was stirred at 0 °C for 2 h and was then added to a solution of TCTA (**2**) (2.22 g, 3 mmol) in a mixed solvent of methylene chloride and DCE at room temperature. The resulting mixture was refluxed overnight and poured in 150 mL of ice water. NaOAc was slowly added to adjust the pH value to ∼7. The aqueous layer was extracted by methylene chloride; the organic layers were combined and dried over Na_2SO_4. The solvent was removed by rotary evaporator, and the crude product was purified through a silica gel flash column with methylene chloride/ethyl acetate (1:1) as eluent to afford 457 mg of **3** as a yellow solid (18%). ^{1}H (300 MHz, $CDCl_3$, δ): 10.17 (s, 3H), 8.72 (d, 3H, J = 1.2 Hz), 8.26 (dd, 3H, J = 7.8 Hz, J = 1.2 Hz), 8.02 (dd, 3H, J = 8.5 Hz, J = 1.5 Hz), 7.64−7.54 (m, 21H), 7.46−7.41 (m, 3H).

TCTA-3CH$_2$OH (4). To a solution of **3** (457 mg, 0.55 mmol) in a mixture of THF (10 mL) and ethanol (10 mL) was added $NaBH_4$ (126 mg, 3.30 mmol) slowly at room temperature. The resulting suspension was stirred for 24 h, and the solvent was rotary evaporated. The crude product was purified through a silica gel flash column with ethyl acetate as eluent to afford a yellowish solid (417 mg, 91%). ^{1}H (300 MHz, $CDCl_3$, δ): 8.18 (d, 6H, J = 7.8 Hz), 7.61−7.45 (m, 24 H), 7.32 (t, 3H, J = 7.8 Hz), 4.92 (s, 6H).

TCTA-TTFV (5). To a stirred solution of **4** (117 mg, 0.14 mmol), 4-trifluorovinyloxy-benzoic acid (107 mg, 0.49 mmol), and 4-(dimethylamino)pyridine (DMAP, 26 mg, 0.20 mmol) in methylene chloride (30 mL) was added 1-[3-(dimethylamino)propyl]-3-ethyl carbodiimde hydrochloride (EDC, 103 mg, 0.54 mmol). The reaction mixture was stirred at room temperature for 20 h. The solvent was evaporated under reduced pressure. The resulting solid was redissolved in methylene chloride, washed with water, dried with Na_2SO_4, and then concentrated. The crude product was purified by column chromatography using methylene chloride/hexane (8:2) as eluent to afford TCTA-TTFV as a slightly yellowish solid (68 mg, 34%). ^{1}H (300 MHz, $CDCl_3$, δ): 8.27 (s, 3H), 8.20 (d, 3H, J = 7.8 Hz), 7.14 (d, 6 H, J = 8.5 Hz), 7.61−7.49 (m, 24 H), 7.35 (t, 3H, J = 7.8 Hz), 7.15 (d, 6H, J = 8.1 Hz), 5.59 (s, 6H). ^{13}C NMR (125 MHz, $CDCl_3$, δ): 169.60, 162.36, 150.53, 145.41, 144.98, 136.74, 136.11, 132.30, 131.52, 131.15, 131.04, 130.34, 129.45, 127.55, 127.16, 125.22, 124.56, 124.30, 119.51, 113.99, 71.79. FTIR (KBr pellet, cm^{-1}): 2950, 1717, 1605, 1509, 1458, 1313, 1267, 1231, 1197, 1162, 1143, 1095, 1014, 805, 765, 745. Anal. Calcd for $C_{84}H_{51}F_9N_4O_9$: C, 70.49; H, 3.59; N, 3.91. Found: C, 70.65; H, 3.77; N, 3.95. ESI-MS (*m*/*z*): 1430.5 (M$^+$).

***p*-Butylphenylhydrazine (6).** Sodium nitrite (11.74 g, 0.17 mol) in water (50 mL) was added over 30 min to an ice-cooled and stirred suspension of 4-*n*-butylaniline (24.30 g, 0.16 mol) in 6 N hydrochloric acid (190 mL). After an additional 15 min, a suspension of tin chloride dihydrate (108.3 g, 0.4 mol) in 6 N hydrochloric acid (190 mL) was added slowly, and the resulting suspension was stirred at 0 °C for 3 h. The solid was filtered and dissolved in a mixture of 40% potassium hydroxide solution (200 mL) and ethyl acetate (200 mL). The organic layer was separated, and the aqueous layer was further extracted with ethyl acetate. The combined organic extracts were washed with 10% hydrochloric acid (120 mL); a solid started to develop in the organic layer. After cooling to 0 °C, the solid was filtered. The organic layer was separated and dried over Na_2SO_4, and the solvent was evaporated. The resulting solid was recrystallized from ethanol to afford a white solid (17.35 g, 54%). ^{1}H (300 MHz, DMSO-d_6, δ): 10.18 (s, 3H), 7.10 (d, 2H, J = 8.4 Hz), 6.92 (d, 2 H, J = 8.7 Hz), 2.51 (t, 2 H, J = 7.5 Hz), 1.50 (pentet, 2H, J = 7.5 Hz), 1.27 (sextet, 2H, J = 7.8 Hz), 0.88 (t, 3H, J = 7.5 Hz).

3-*n*-Butyl-5,6,7,8-9*H*-carbazole (7). *p*-Butylphenylhydrazine (8.31 g, 40 mmol), cyclohexanone (4.32 g, 44 mmol), and acetic acid (16 g) were refluxed for 1 day. The mixture was then cooled to 5 °C. The resulting solid was filtered, washed with water, and recrystallized from ethanol to give the title compound (5.64 g, 62%). ^{1}H (300 MHz, $CDCl_3$, δ): 7.57 (s, 1H), 7.20 (d, 1H, J = 8.4 Hz), 6.98 (d, 1H, J = 8.1 Hz), 2.73 (t, 6 H, J = 7.5 Hz), 1.92 (d, 4H, J = 5.4 Hz), 1.67 (pentet, 2H, J = 7.2 Hz), 1.41 (sextet, 2H, J = 7.2 Hz), 0.93 (t, 3H, J = 7.5 Hz).

3-*n*-Butyl-9*H*-carbazole (8). A mixture of **7** (5.64 g, 24.8 mmol) and 10 wt % palladium on activated carbon (1.09 g) were heated to 250−260 °C until the evolution of the hydrogen ceased. The mixture was then extracted with THF, and the solvent was evaporated. The solid was recrystallized from ethanol to give **8** as a slightly brown solid (3.85 g, 69%).^{1}H (300 MHz, DMSO-d_6, δ): 8.03 (d, 1H, J = 7.8 Hz), 7.86 (s, 1H), 7.40 (d, 1H, J = 8.1 Hz), 7.31 (t, 6H, J = 7.5 Hz), 7.17 (dd, J = 8.4 Hz, J = 1.8 Hz), 7.08 (t, 1H, J = 8.1 Hz), 2.69 (t, 2H, J = 7.2 Hz), 1.60 (pentet, 2H, J = 7.5 Hz), 1.31 (sextet, 2H, J = 7.5 Hz), 0.89 (t, 3H, J = 7.5 Hz).

Bu-TCTA (9). To a stirred mixture of tris(4-iodophenyl)amine (1.87 g, 3.0 mmol), 3-*n*-butyl-9*H*-carbazole (2.68 g, 12.0 mmol), copper powder (86 mg, 1.35 mmol), and potassium carbonate (2.49 g, 18.0 mmol) was added nitrobenzene (10 mL) under nitrogen. The mixture was refluxed for 3 d. The hot solution was filtered, and the filtrate was added dropwise to methanol. The precipitate was filtered and washed successively with methanol and water. It was then redissolved in benzene and purified through a silica gel column with a gradient solvent of hexane to hexane/benzene (4:1) as eluent to afford a slightly brown solid (943 mg, 34%). ^{1}H (300 MHz, $CDCl_3$, δ): 8.13 (dd, 3H, J = 7.5 Hz, J = 0.9 Hz), 7.96 (d, 3H, J = 0.9 Hz), 7.58−7.40 (m, 21 H), 7.29 (t, 6H, J = 6.6 Hz), 2.83 (t, 6H, J = 7.8 Hz), 1.73 (pentet, 6H, J = 7.8 Hz), 1.43 (sextet, 6H, J = 7.5 Hz), 0.97 (t, 9H, J = 7.2 Hz). ^{13}C NMR (125 MHz, $CDCl_3$, δ): 150.36, 145.22, 143.66, 139.01, 138.69, 137.37, 137.02, 134.14, 132.16, 130.80, 130.60, 129.81, 129.38, 124.35, 123.68, 113.52, 39.79, 38.60, 26.50, 18.15.

Bu-TCTA-3I (10). To a stirred mixture of Bu-TCTA (935 mg, 1.03 mmol) and NIS (811 mg, 3.60 mmol) in chloroform (6 mL) was added acetic acid (4 mL) at room temperature under the exclusion of light. The solution was stirred overnight at room temperature. The reaction mixture was then poured in water, washed with sodium thiosulfate, and extracted with methylene chloride. The combined methylene chloride layers were washed with water, dried with Na_2SO_4, and concentrated. The crude product was purified through a silica gel column with hexane/methylene chloride (6:4) as eluent to afford a slightly brown solid (1.30 g, 98%). ^{1}H (300 MHz, $CDCl_3$, δ): 8.44 (s, 3H), 7.89 (s, 3H), 7.66−7.50 (m, 21H), 7.29−7.28 (m, 3H) 2.83 (t, 6H, J = 7.8 Hz), 1.69 (pentet, 6H, J = 7.5 Hz), 1.41 (sextet, 6H, J = 7.2 Hz), 0.96 (t, 9H, J = 7.8 Hz).

Bu-TCTA-3CH$_2$OH (12). To a solution of **10** (1.38 g, 1.07 mmol) in dry THF (50 mL) was added dropwise *n*-butyllithium (1.5 mL, 2.5 M in hexane) at −78 °C under a nitrogen atmosphere. The solution was stirred at −78 °C for 2 h, followed by the addition of DMF (0.40 mL, 2.1 mmol). The resulting reaction mixture was slowly warmed to room temperature and stirred for an additional 2 h. The reaction was quenched with water, and the THF solvent was evaporated under vacuo. The residue was extracted with methylene chloride, and the combined organic layers were washed with water, dried with Na_2SO_4, and concentrated. The crude compound **11** was reduced by $NaBH_4$ in a mixed solvent of ethanol (10 mL) and benzene (10 mL). The resulting suspension was stirred for 24 h, and solvent was removed by rotary evaporator. The crude product was purified through a silica gel column with methylene chloride/ethyl acetate (9:1) as eluent to afford **12** in 31% yield. ^{1}H (300 MHz, $CDCl_3$, δ): 8.17 (s, 3H), 7.98 (s, 3H), 7.60−7.44 (m, 21H), 7.29 (dd, 3H, J = 8.4 Hz, J = 1.5 Hz), 4.90 (s, 6H), 2.84 (t, 6H, J = 7.8 Hz), 1.74 (pentet, 6H, J = 7.2 Hz), 1.45 (sextet, 6H, J = 7.5 Hz), 1.26 (t, 9H, J = 6.9 Hz). ^{13}C NMR (125 MHz, $CDCl_3$, δ): 150.28, 144.80, 143.79, 138.85, 137.01, 136.51, 132.04, 130.95, 129.53, 129.36, 127.50, 127.35, 123.78, 123.37, 113.89, 113.65,

Scheme 1. Synthesis of TCTA-TTFV

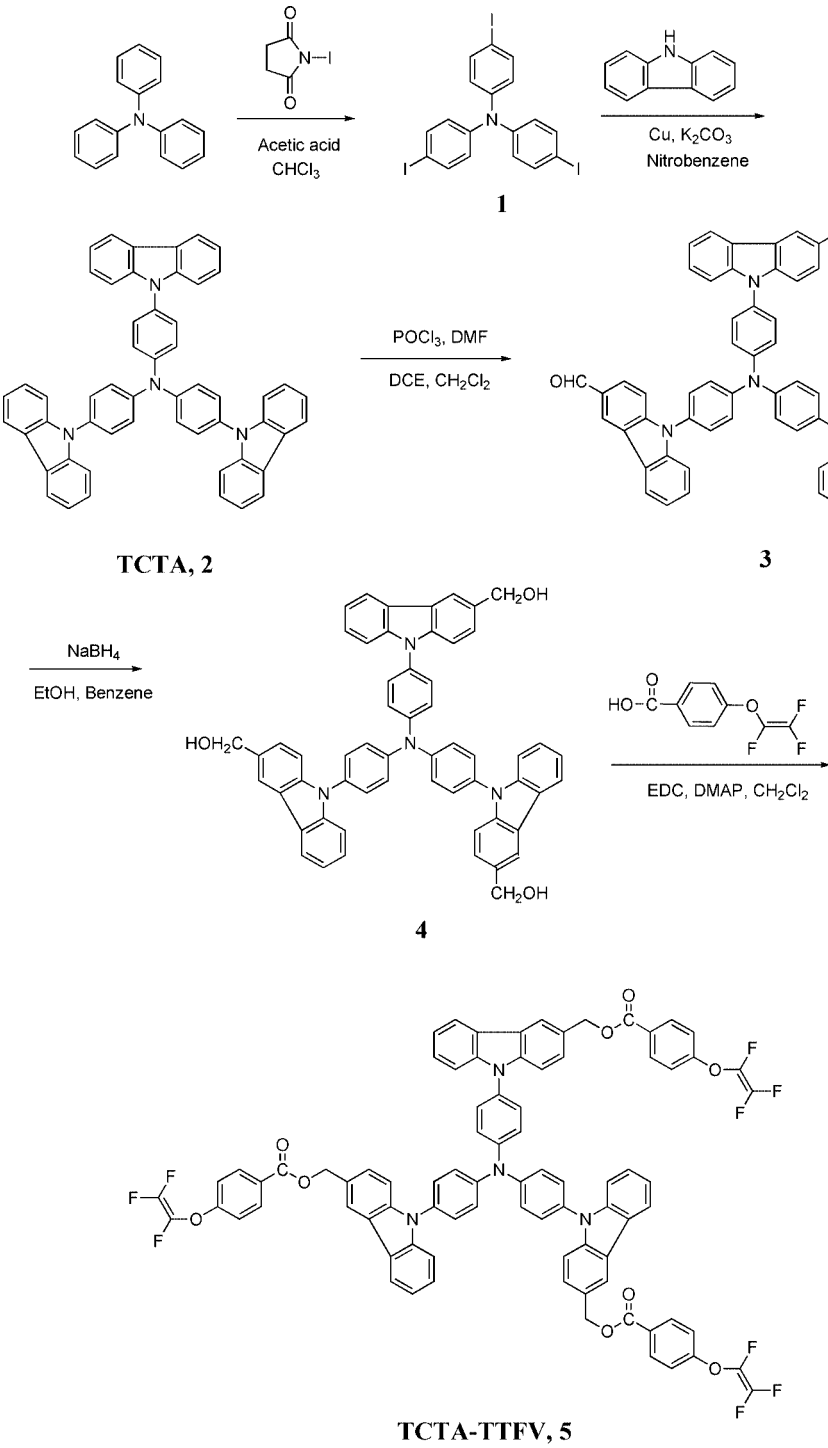

70.05, 39.73, 38.53, 26.45, 18.11. FTIR (KBr pellet, cm^{-1}): 2950, 2921, 2857, 1606, 1510, 1464, 1309, 1234, 1190, 1014, 879, 807. ESI-MS (*m*/*z*): 998.7 (M^+).

Bu-TCTA-TTFV (13). To a solution mixture of **12** (255 mg, 0.26 mmol), 4-trifluorovinyloxy-benzoic acid (184 mg, 0.84 mmol), and DMAP (32 mg, 0.26 mmol) in methylene chloride (10 mL) was added EDC (184 mg, 0.96 mmol). The reaction mixture was stirred at room temperature for 20 h. The solvent was evaporated under reduced pressure. The solid was redissolved in methylene chloride, washed with water, dried with Na_2SO_4, and then concentrated. The crude product was purified by column chromatography using methylene chloride/hexane (4:1) as eluent to afford Bu-TCTA-TTFV as a slightly yellowish solid (282 mg, 68%). ^1H (300 MHz, $CDCl_3$, δ): 8.25 (s, 3H), 8.14 (d, 6H, $J = 9.1$ Hz), 7.80 (s, 3H), 7.60−7.51 (m, 18H), 7.44 (d, 3H, $J = 8.4$ Hz), 7.33−7.30 (m, 3H), 7.15 (d, 6H, $J = 8.1$ Hz), 5.58 (s, 6H), 2.85 (t, 6H, $J = 7.2$ Hz), 1.74 (pentet, 6H, $J = 7.2$ Hz), 1.46 (sextet, 6H, $J = 7.8$ Hz), 1.01 (t, 9H, $J = 7.2$ Hz).^{13}C NMR (125 MHz, $CDCl_3$, δ): 169.62, 162.34, 150.64, 150.39, 145.15, 143.87, 139.03, 136.94, 136.11, 132.13, 131.24, 131.19, 131.13, 130.87, 129.39, 127.53, 127.24, 125.20, 123.86, 119.50, 113.91, 113.69, 71.88, 39.74, 38.54, 26.45, 18.09. FTIR (KBr pellet, cm^{-1}): 2950, 2926, 2857, 1719, 1606, 1509, 1467, 1316, 1269, 1200, 1165, 1141, 1097, 1014, 809, 764. Anal. Calcd for $C_{96}H_{75}F_9N_4O_9$: C, 72.08; H, 4.73; N, 3.50. Found: C, 71.99; H, 4.95; N, 3.43. ESI-MS (*m*/*z*): 1599.6 (M^+).

TCTA-2I (14). To a stirred mixture of TCTA (1.40 g, 1.89 mmol) and NIS (893 mg, 3.97 mmol) in chloroform (20 mL) was added acetic acid (8 mL) at room temperature under the exclusion

Scheme 2. Synthesis of Bu-TCTA

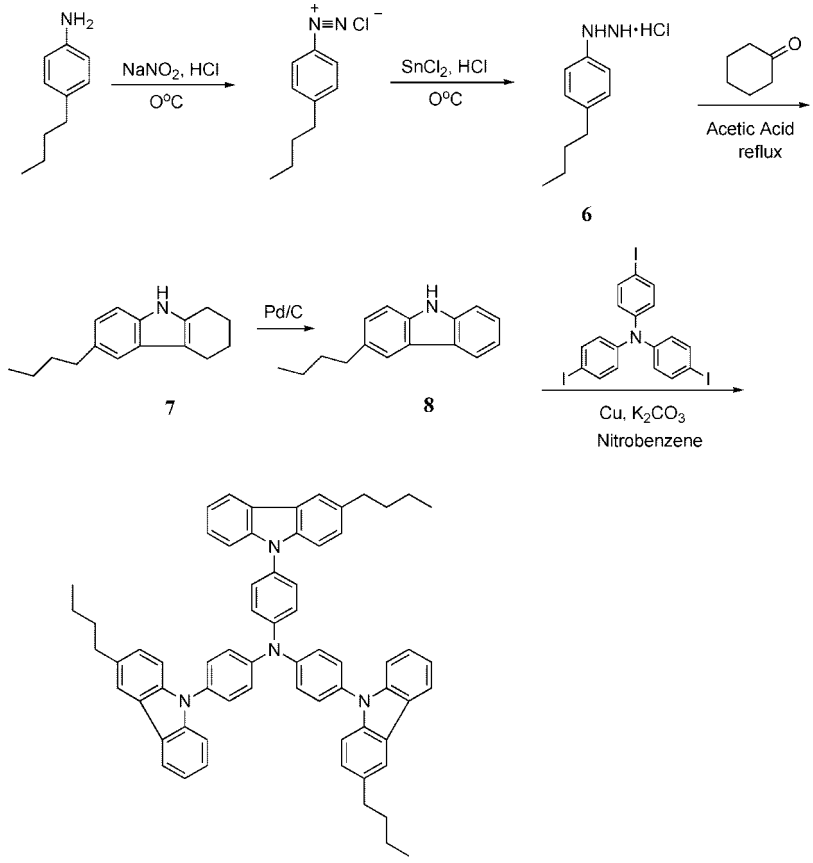

Bu-TCTA, 9

of light. The solution was stirred overnight at room temperature. The reaction mixture was poured in water, washed with sodium thiosulfate, and extracted with methylene chloride. The combined methylene chloride layers were washed with water, dried with Na_2SO_4, and concentrated. The crude product was purified through a silica gel column with hexane/methylene chloride (6:4) as eluent to afford a slightly brown solid (1.36 g, 72%). ^{1}H (300 MHz, $CDCl_3$, δ): 8.49 (s, 2H, J = 1.8 Hz), 8.19 (d, 2H, J = 7.8 Hz), 8.12 (d, 2H, J = 7.8 Hz), 7.71 (dd, 2H, J = 8.7 Hz, J = 1.8 Hz), 7.62−7.45 (m, 20H), 7.37−7.31 (m, 6H).

TCTA-2CHO (15). To a solution of **14** (834 mg, 0.84 mmol) in dry THF (30 mL) was added dropwise *n*-butyllithium (0.74 mL, 2.5 M in hexane) at −78 °C under a nitrogen atmosphere. The solution was stirred at −78 °C for 45 min, followed by the addition of DMF (0.16 mL, 2.1 mmol). The resulting reaction mixture was slowly warmed to room temperature and stirred overnight. The reaction was quenched with water, and the THF solvent was evaporated under vacuo. The residue was extracted with methylene chloride. The combined organic layers were washed with water, dried with Na_2SO_4, and concentrated. The crude product was purified through a silica gel column with a gradient solvent of hexane/methylene chloride (1:1) to methylene chloride as eluents to afford a yellow solid (384 mg, 57%). ^{1}H (300 MHz, $CDCl_3$, δ): 10.17 (s, 2H), 8.72 (s, 2H), 8.25 (d, 2H, J = 7.8 Hz), 8.20 (d, 2H, J = 7.8 Hz), 8.02 (dd, 2H, J = 8.4 Hz, J = 1.2 Hz), 7.67−7.40 (m, 24H), 7.34 (t, 2H, J = 6.6 Hz).

TCTA-2CH$_2$OH (16). To a solution of **15** (384 mg, 0.48 mmol) in a mix solvent of benzene (10 mL) and ethanol (10 mL) was added $NaBH_4$ (109 mg, 2.88 mmol) at room temperature. The resulting suspension was stirred for 24 h, and solvent was removed by rotary evaporator. The crude product was purified through a silica gel column with methylene chloride/ethyl acetate (9:1) as eluent to afford a white solid (369 mg, 96%). ^{1}H (300 MHz, $CDCl_3$, δ): 8.18 (d, 6H, J = 7.5 Hz), 7.63−7.45 (m, 24H), 7.34 (t, 4H, J = 6.9 Hz), 4.92 (s, 4H). ^{13}C NMR (125 MHz, $CDCl_3$, δ): 150.47, 145.34, 144.98, 144.64, 136.76, 132.31, 132.22, 130.16, 130.00, 129.72, 129.49, 129.37, 127.52, 127.39, 127.27, 124.47, 124.13, 124.02, 123.42, 113.96, 113.84, 70.00. FTIR (KBr pellet, cm^{-1}): 3049, 2866, 1623, 1601, 1510, 1455, 1311, 1229, 1015, 806, 748, 724. ESI-MS (*m*/*z*): 800.6 (M$^+$).

TCTA-BVB (17). To a solution of **16** (530 mg, 0.69 mmol) was added sodium hydride (53 mg, 2.1 mmol) at room temperature under nitrogen. After stirring for 2.5 h, 4-vinylbenzyl chloride (427 mg, 2.8 mmol) was added, and the mixture was stirred overnight. The suspension was poured in water and extracted with methylene chloride. The extracts were dried with Na_2SO_4 and concentrated. The crude product was purified by column chromatography using hexane/methylene chloride (3:2) as eluent to afford TCTA-BVB as a slightly yellowish solid (371 mg, 52%). ^{1}H (300 MHz, $CDCl_3$, δ): 8.21 (d, J = 6.9 Hz, 6H), 7.64−7.33 (m, 36H), 6.77 (q, 2H, J = 10.8 Hz, J = 6.9 Hz), 5.80 (d, 2H, J = 17.7 Hz), 5.29 (d, 2H, J = 10.5 Hz), 4.80 (s, 4H), 4.65 (s, 4H). ^{13}C NMR (125 MHz, $CDCl_3$, δ): 150.47, 150.43, 145.33, 145.02, 144.72, 142.14, 141.04, 140.64, 136.92, 136.85, 133.89, 132.33, 132.25, 132.15, 130.51, 130.33, 130.10, 130.02, 129.77, 129.47, 129.40, 127.45, 127.41, 127.34, 124.51, 124.44, 124.34, 124.11, 124.03, 117.84, 113.95, 113.87, 76.69, 75.61. FTIR (KBr pellet, cm^{-1}): 3044, 2847, 1623, 1601, 1509, 1453, 1360, 1312, 1231, 1078, 1015, 910, 828, 768, 748, 724. Anal. Calcd for $C_{74}H_{56}N_4O_2$: C, 86.02; H, 5.46; N, 5.42. Found: C, 85.95; H, 5.54; N, 5.37. ESI-MS (*m*/*z*): 1032.7 (M$^+$).

Polymer Light-Emitting Diode Device Fabrication and Characterization. The PLEDs were fabricated on precleaned and O_2-plasma-treated ITO-covered glass substrates. After the plasma treatment, the substrates were moved into a glovebox, and all of the subsequent film-forming processes were performed in it under argon protection. For the LED with double HTLs, the first HTL ($\sim$ 30 nm) was formed by spin-coating the PS-TPD-TFV solution onto ITO and then thermally cross-linking it on a hotplate at 235 °C for 40 min. A robust uniform film with good solvent resistance can thus be formed, and we refer to this cross-linked hole-transport

Scheme 3. Synthesis of Bu-TCTA-TTFV

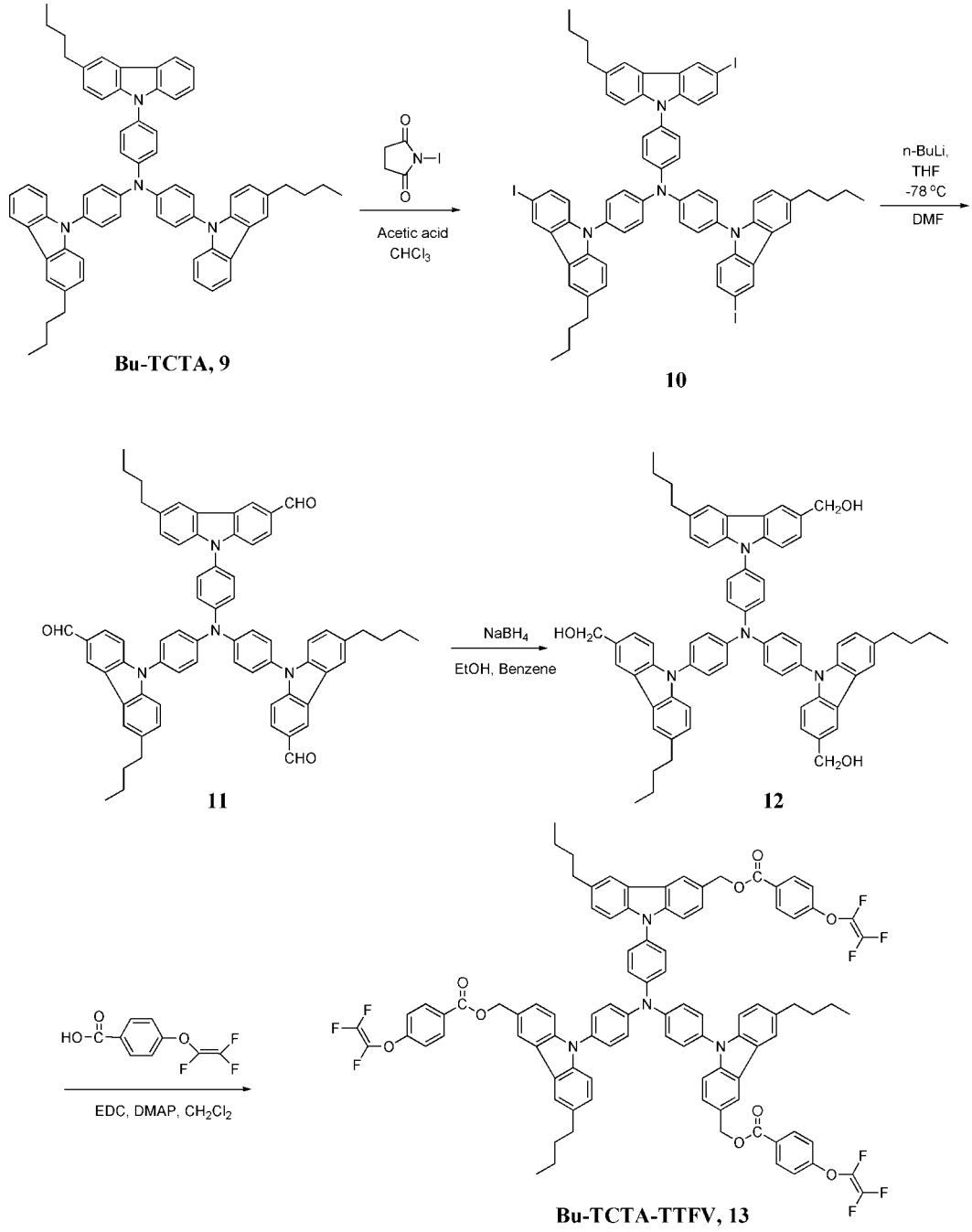

network as PS-TPD-PFCB. On top of this layer, the second HTL (~ 20 nm) was formed via spin coating from either TCTA-TTFV or Bu-TCTA-TTFV and thermally cross-linked at 225 °C for 40 min or from TCTA-BVB solution and cross-linked at 180 °C for 30 min. A 40-nm-thick EML was then spin coated on top of the HTLs. In a vacuum below 1×10^{-6} torr, a layer of TPBI with a thickness of 25 nm was sublimed. Cesium fluoride (CsF) with a thickness of 1 nm and Al with a thickness of 200 nm were evaporated subsequently as cathode.

The performance test was carried out at room temperature in air without encapsulation. Current density−voltage ($J-V$) characteristics were measured on a Hewlett-Packard 4155B semiconductor parameter analyzer. The PL and EL spectra were recorded by a spectrometer (Instaspec IV, Oriel). The light power of the EL emission was measured using a calibrated Si-photodiode and a Newport 2835-C multifunctional optical meter. Photometric units (cd/m^2) were calculated using the forward output power together with the EL spectra of the devices under the assumption of the emission's Lambertian space distribution.

Results and Discussion

Synthesis and Characterization. 4,4′,4″-Tris(*N*-carbazolyl)-triphenyl amine (TCTA, **2**) was synthesized through a two-step reaction from triphenylamine: the triiodation of tripheylamine with NIS in acetic acid, followed by the Ullmann reaction between the corresponding amine triiodide and carbazole in the presence of copper and potassium carbonate (Scheme 1).[18,35] The direct formylation of TCTA with $POCl_3$/DMF under the Vilsmeier condition using DCE as the solvent gave triformylated TCTA (**3**). The reduction of the resulting TCTA trialdehyde with sodium borohydride afforded the trihydroxy-containing TCTAs (**4**) in quantitative yields. Tris(trifluorovinyl ether)-containing TCTA (TCTA-TTFV, **5**) was obtained by condensing

Scheme 4. Synthesis of TCTA-BVB

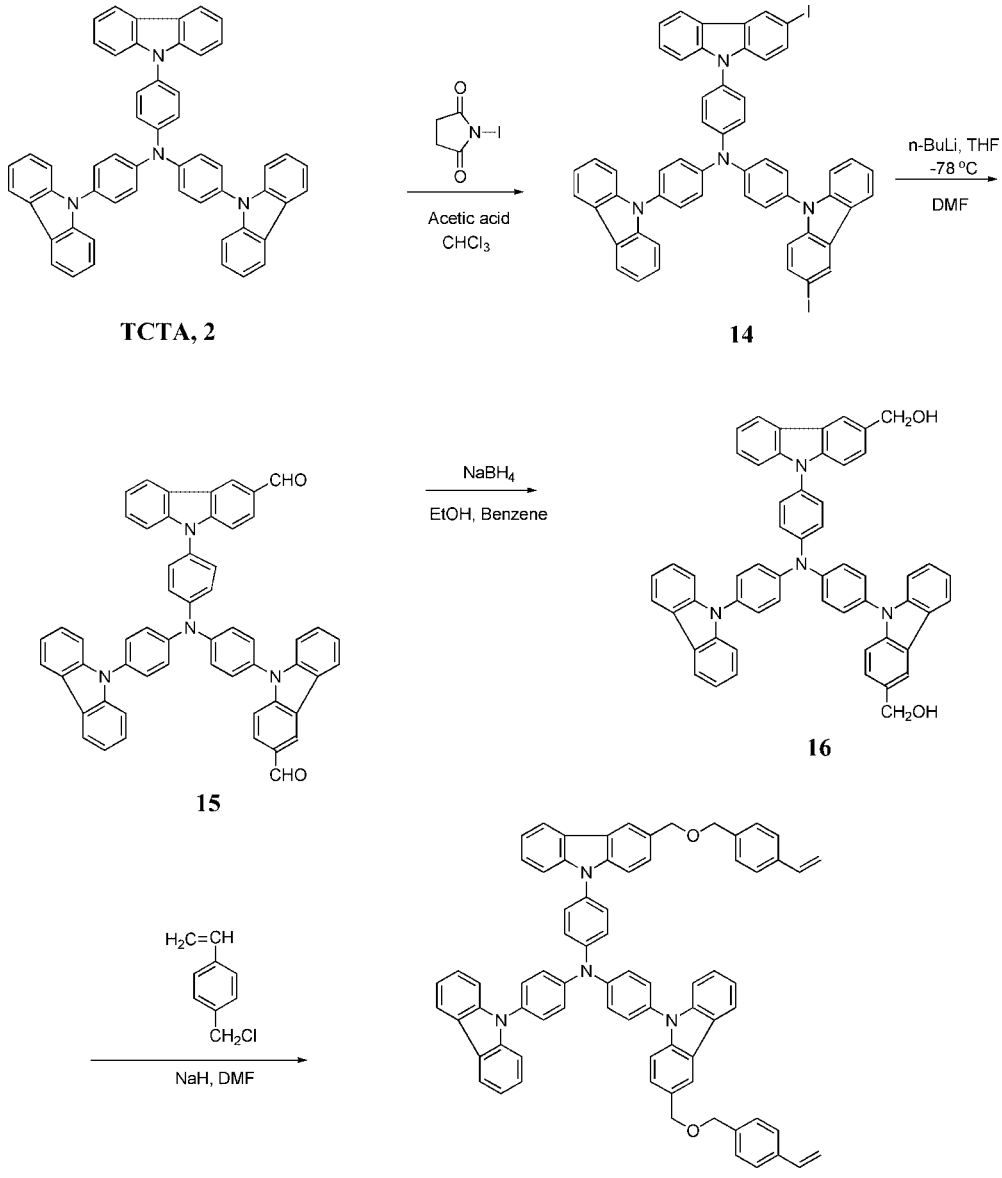

TCTA, 2 **14** **15** **16** **TCTA-BVB, 17**

the trihydroxyl-TCTA (**4**) with 4-trifluorovinyloxy-benzoic acid using 1-[3-(dimethylamino)propyl]-3-ethylcarbodiimde hydrochloride (EDC) and DMAP as the reagents.

Because TCTA tends to crystallize at 190 °C, which is far below the [2 + 2] cycloaddition polymerization temperature of trifluorovinyl ethers (~235 °C),[36] the flexible *n*-butyl groups were introduced to prevent it from crystallizing during thermal curing. The butyl-substituted TCTA, 4,4′,4″-tris(*N*-3-*n*-butylcarbazolyl)triphenylamine (Bu-TCTA**, 9**) was synthesized through the Ullmann reaction between tris(4-iodophenyl)amine and 3-*n*-butyl-9*H*-carbazole, which was obtained by the dehydrogenation of 3-*n*-butyl-5,6,7,8−9*H*-carbazole. 3-*n*-Butyl-5,6,7,8−9*H*-carbazole was synthesized from cyclohexanone and *n*-butylphenylhydrazine hydrochloride under acidic conditions (Scheme 2).[37] The direct formylation of TCTA with $POCl_3$/DMF under the Vilsmeier condition gave mono-, di-, and triformylated TCTA mixtures in poor yield, which may be due to the poor solubility of TCTA in DCE, a common solvent used for the Vilsmeier reaction. Therefore, a two-step reaction procedure was adopted to make Bu-TCTA trialdehyde (**11**). Bu-TCTA (**9**) was first iodinated by three equivalents of NIS; then, the formyl groups were introduced by lithiating Bu-TCTA triiodide with *n*-BuLi, followed by quenching with DMF. The reduction of the resulting Bu-TCTA trialdehyde, followed by the condensation with 4-trifluorovinyloxy-benzoic acid gave tris(trifluorovinyl ether)-containing Bu-TCTA (Bu-TCTA-TTFV, **13**) (Scheme 3).

The TCTA dialdehyde (**15**) was obtained according to the same two-step reaction procedure as that described above for Bu-TCTA trialdehyde (**11**). The TCTA dialdehyde (**15**) was then reduced by the sodium borohydride. The etherification between the resulting dihydroxy TCTA (**16**) and 4-vinylbenzyl chloride with sodium hydride as base yielded bis(vinylbenzyl ether)-containing TCTA (TCTA-BVB, **17**) (Scheme 4).

The chemical structures of all TCTA derivatives were confirmed through ^{1}H NMR, ^{13}C NMR, elemental analysis, and mass spectroscopy.

Electrochemical Properties. The ionization potentials of the TCTA derivatives in DCE were determined by cyclic voltammetry. All of the compounds exhibit reversible oxidative behavior with the onset potentials at ~0.55 V, which is similar to that of TCTA. This indicates that the derivatization of TCTA

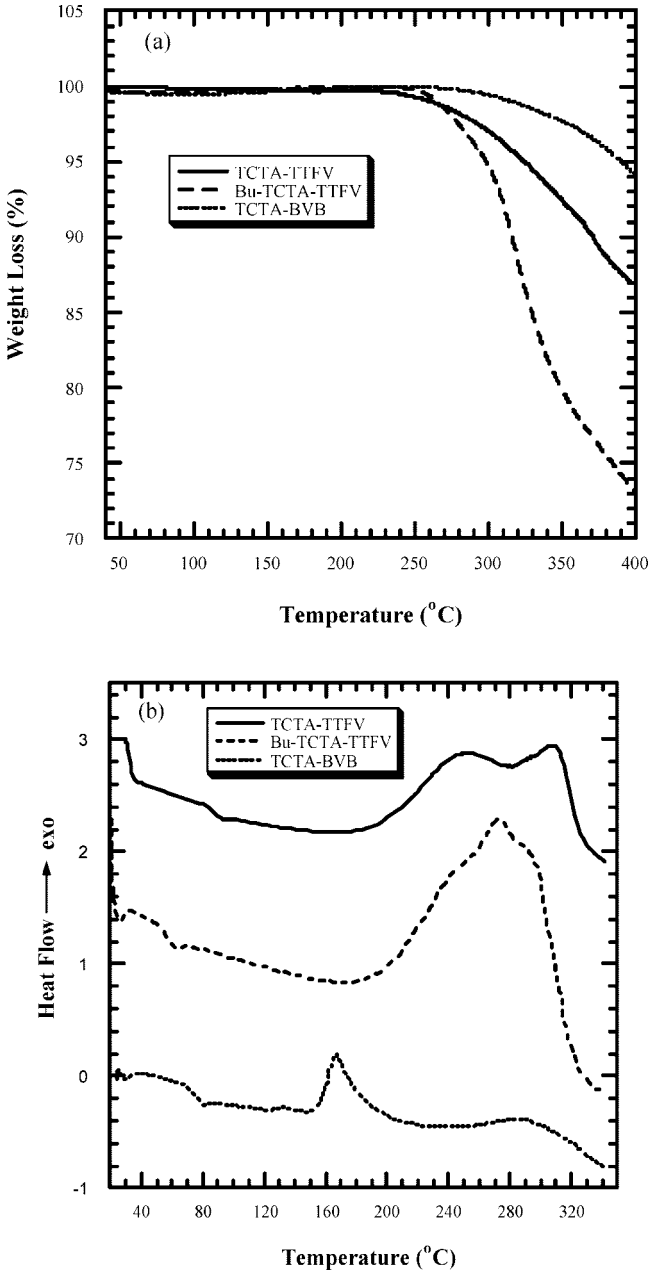

Figure 3. (a) TGA and (b) DSC studies of the polymerization reactions of TCTA derivatives with trifluorovinyl ether or vinylbenzyl ether functional groups.

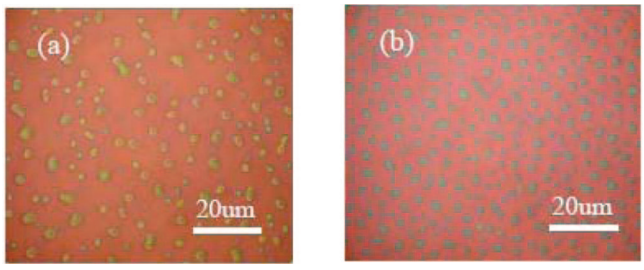

Figure 4. Optical micrographs of TFV-functionalized TCTA on PS-TPD-PFCB layer after thermal curing at 225 °C for 30 min. (a) TCTA-PFCB and (b) Bu-TCTA-PFCB.

by TFV or VB groups does not affect the electronic property of the TCTA. The HOMO energy level of the TCTA derivatives was assigned to be −5.7 eV according to the data reported for TCTA.[18]

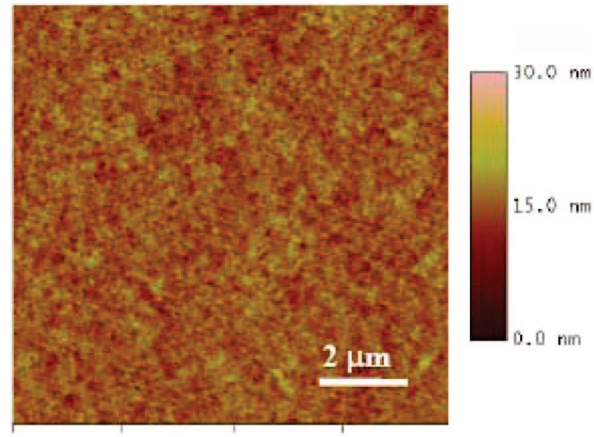

Figure 5. Tapping mode AFM images of TCTA-BVB on PS-TPD-PFCB layer after thermal curing at 180 °C for 30 min.

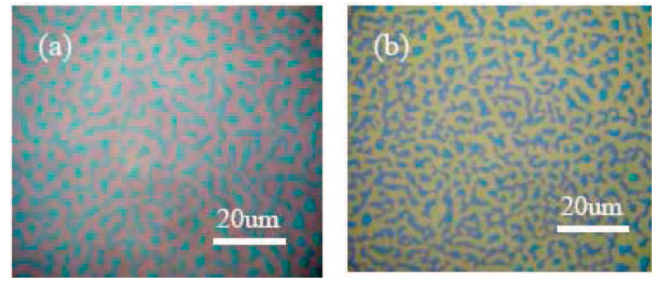

Figure 6. Optical micrographs of TFV-functionalized TCTA on ITO substrate after thermal curing at 225 °C for 30 min. (a) TCTA-PFCB and (b) Bu-TCTA-PFCB.

Table 1. PLED Device Performance with Single HTL Having the Structure of ITO/HTL/PVK−FIr6 (10 wt %)/TPBI/CsF/Al

HTL	V_{on} (V)[a]	Q_{max} (%)[b]	B (cd/m^2)[c]	V (V)[d]	LE_{max} (cd/A)[e]	B_{max} (cd/m^2)[f]	Q (%)[g]
PEDOT	5.5	1.98	753	8.0	3.66	13 800	1.48
PS-TPD-PFCB	7.0	1.24	28.2	8.5	2.39	3070	0.92
TCTA-PFCB	6.0	2.28	100	8.0	4.21	6000	2.28

[a] Turn-on voltage. [b] Maximum external quantum efficiency. [c] Brightness at the maximum efficiency. [d] Voltage at the maximum efficiency. [e] Maximum luminous efficiency. [f] Maximum brightness. [g] External quantum efficiency at 100 cd/m^2.

Thermal Properties. All TCTA derivatives exhibit high thermal stability, with only ∼5% weight loss observed at temperatures of up to 300 °C by TGA, indicating their stability against thermal degradation (Figure 3a). Among three compounds, TCTA-BVB shows the best stability. The optimal cross-linking conditions were determined by DSC through heating TCTA derivatives to 350 °C at 10 °C/min (Figure 3b). Upon heating, TCTA-TTFV exhibits a glass-transition temperature (T_g) of 88 °C, whereas Bu-TCTA-TTFV shows a lower T_g of 55 °C because of the presence of flexible alkyl chains. The T_g of TCTA-BVB is measured to be 77 °C. After further heating above T_g, both TFV-containing TCTAs reveal an exothermic onset of ∼195 °C (which is the typical dimerization temperature for trifluorovinyl ether) and another exothermic peak at 252 °C.[28,38,39] However, at this temperature, both compounds start to decompose, as revealed by their TGA measurements. TCTA-BVB begins to polymerize at a much lower temperature (∼150 °C) with an exothermic peak at 170 °C, which is consistent with the autopolymerization of styrene.[40] To ensure a fast and high-yield cross-linking process, the cyclopolymerization of the TFV-containing TCTA was performed under an inert atmosphere at 225 °C for 30 min, whereas the polymerization of TCTA-BVB was conducted at 180 °C for 30 min to form

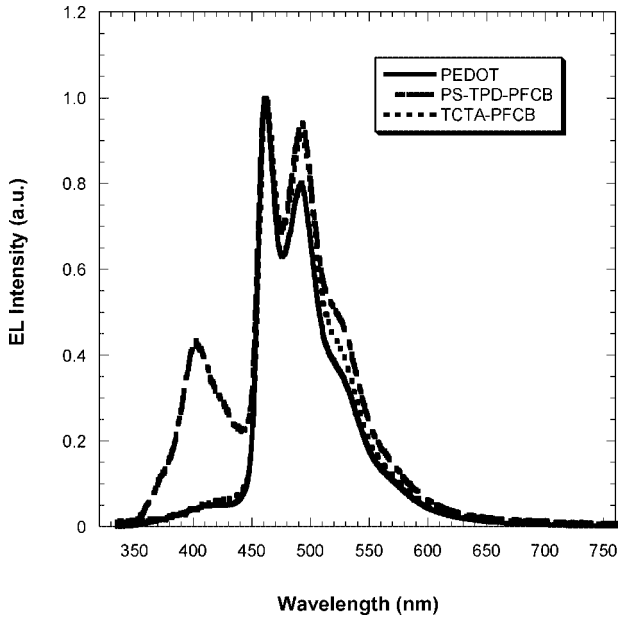

Figure 7. EL spectra of the single HTL PLED devices with the device configuration of ITO/HTL/PVK−FIr6 (10 wt %)/TPBI/CsF/Al.

Table 2. PLED Device Performance with Double HTLs Having the Structure of ITO/PS-TPD-PFCB/HTL2/PVK−FIr6 (10 wt %)/TPBI/CsF/Al

HTL2	V_{on} (V)[a]	Q_{max} (%)[b]	B (cd/m^2)[c]	V (V)[d]	LE_{max} (cd/A)[e]	B_{max} (cd/m^2)[f]	Q (%)[g]
TCTA-PFCB	6.6	3.67	805	10.4	8.34	12 500	2.02
Bu-TCTA-PFCB	8.2	3.47	851	13.0	7.56	10 600	2.53
x-TCTA-BVB	6.0	3.17	441	9.5	6.60	17 400	2.77

[a] Turn-on voltage. [b] Maximum external quantum efficiency. [c] Brightness at the maximum efficiency. [d] Voltage at the maximum efficiency. [e] Maximum luminous efficiency. [f] Maximum brightness. [g] External quantum efficiency at 100 cd/m^2.

the TCTA networks. We designate the cross-linked forms of TCTA-TTFV, Bu-TCTA-TTFV, and TCTA-BVB as TCTA-PFCB, Bu-TCTA-PFCB, and x-TCTA-BVB, respectively.

The films of TCTA derivatives with a thickness of ∼20 nm were spin coated from their DCE solutions onto the glass substrates. After thermal curing, we investigated the solubility of the cross-linked films by measuring their UV−vis spectra before and after washing with various organic solvents, such as chlorobenzene, DCE, toluene, and chloroform, which are the common solvents used for spin coating light-emitting polymers. The unchanged UV−vis spectra indicate that these polymers possess suitable solvent resistance that can be used for multilayer integration in PLEDs.

Morphology Study. For PLED application, it is crucial to obtain high-quality thin films with minimum defects such as aggregates or pinholes, which often contribute to reduced lifetime and performance of the device. The morphology of double HTLs with 20-nm-thick TCTA derivatives spin coated onto 30-nm-thick cross-linked PS-TPD-PFCB before and after thermal curing were investigated using tapping mode atomic force microscopy (AFM) and optical microscopy. The first HTL from PS-TPD-PFCB is very smooth with an rms roughness of ∼0.63 nm, indicating the effective planarization of the ITO surface by the PS-TPD-PFCB film. The as-spun films of three TCTA derivatives on PS-TPD-PFCB are also quite smooth with rms roughness of <1 nm. However, the surface roughness dramatically increases after thermal curing at 225 °C for 30 min for TFV-containing TCTAs. As shown in Figure 4a,b, there are many islands formed after cross-linking. The heights of these islands in TCTA-PFCB are greater than 300 nm, which is >100

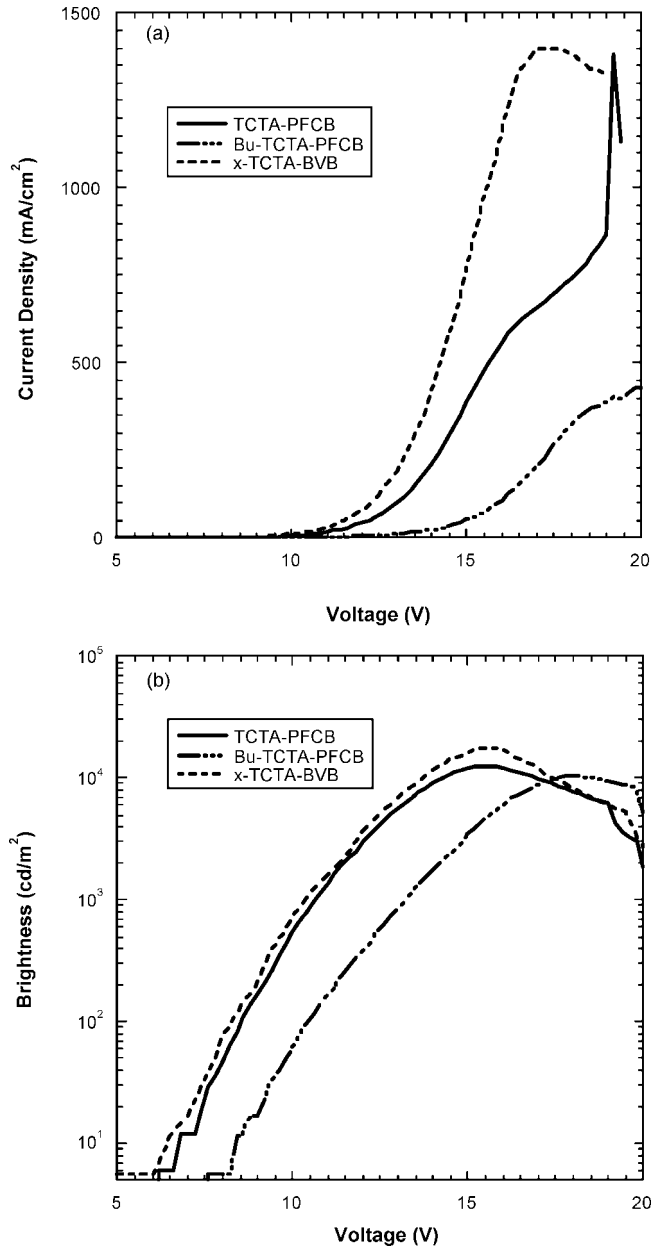

Figure 8. (a) Current density−voltage and (b) brightness−voltage characteristics of the PLED devices (ITO/PS-TPD-PFCB/HTL2/PVK−FIr6 (10 wt %)/TPBI/CsF/Al) with double HTLs.

nm higher than those observed for Bu-TCTA-PFCB (measured by AFM). In sharp contrast, the cross-linked TCTA-BVB film (which was cured at 180 °C) shows only a slightly increased roughness compared with its film before cross-linking. The rms roughness of this double-layer film is 1.62 nm, indicating good cohesion between the cross-linked TCTA-BVB and PS-TPD-PFCB layers (Figure 5). There may be two reasons that contribute to the island formation in TFV-containing TCTAs. One reason may be due to the dewetting between the top TCTA-PFCB layer and the bottom PS-TPD-PFCB layer. Because of the high fluoro content in the TFV-functionalized TCTAs, the surface energy of these TCTA layers is lower than that of PS-TPD-PFCB. As a result, the cohesion between TCTA-PFCB/PS-TPD-PFCB or Bu-TCTA-PFCB/PS-TPD-PFCB interfaces is quite weak, causing the dewetting between these two layers during heating. Another possible reason may be due to the thermal-induced crystallization of TCTA moieties during the high-temperature polymerization process.

To differentiate these two mechanisms, we have also investigated the effect of crystallization on the morphology of 20-nm-thick TFV-functionalized TCTA films on bare ITO substrates. Before curing, smooth and featureless films were observed by AFM over a 30 × 30 μm scanned area; the rms roughness is 0.63 and 0.55 nm for TCTA-TTFV and Bu-TCTA-TTFV films, respectively. After curing at 225 °C, which is well above the TCTA crystallization temperature (190 °C), for 30 min, TCTA crystallization/aggregation can be clearly seen under optical microscope. The surface of these films became very rough, and the spinodal morphologies are observed for both TCTA-PFCB and Bu-TCTA-PFCB, as illustrated in Figure 6. It is also quite surprising to find out that the introduction of flexible alkyl chains on Bu-TCTA-TTFV does not suppress the formation of aggregates. Therefore, the height variations and rougher topographies exhibited across the surface of TFV-functionalized TCTAs on top of PS-TPD-PFCB are believed to be the combined effects of TCTA crystallization and incompatibility between these two layers.

Polymer Light-Emitting Diode Devices Using Single Hole-Transporting Layer. The performance of blue electrophosphorescent PLEDs employing single HTL with the device configuration of ITO/HTL/PVK−FIr6 (10 wt %)/TPBI/CsF/Al was investigated and summarized in Table 1. Here the commercial PEDOT/PSS (60 nm), PS-TPD-PFCB (30 nm), and TCTA-PFCB (20 nm) were all used to compare their suitability as HTL for blue electrophosphorescent LEDs systematically. Figure 7 shows the EL spectra of the PLEDs with single HTL. By using PEDOT/PSS as HTL, the blue emission band from the FIr6 dopant can be observed. However, when PS-TPD-PFCB was used as HTL, another shorter wavelength emission band was detected, which is due to the emission from the TPD units on PS-TPD-PFCB. The observed TPD emission is caused by insufficient electron/exciton confinement by the PS-TPD-PFCB layer. The injected electrons climb over the energy barrier between the PS-TPD-PFCB and PVK−FIr6 interface to form excitons in TPD. The purity of emission can be improved by employing a TCTA-PFCB layer as HTL because it possesses a higher LUMO energy than PS-TPD-PFCB, thus providing better electron blocking capability. In addition, the larger bandgap (3.4 eV) of TCTA-based hole-transporting materials can better confine the excitons within the EML. As a result, the device emission is solely from the blue phosphor dopants. The enhanced electron/exciton blocking capacity of TCTA-PFCB layer also results in higher external quantum efficiency compared with that of the devices based on PEDOT/PSS (Table 1). However, the maximum brightness obtained from TCTA-PFCB-based PLED is only about half of that of the device made from PEDOT/PSS as HTL. The low brightness is the result of less-efficient hole injection due to the higher energy barrier between ITO and TCTA-PFCB (1.0 vs 0.5 eV for PEDOT/PSS) (Figure 2).

Polymer Light-Emitting Diode Devices Using Double Hole-Transporting Layers. The PLEDs with double HTLs (ITO/PS-TPD-PFCB/TCTA-derivative/PVK−FIr6 (10 wt %)/TPBI/CsF/Al) were fabricated for studying the function of TCTA derivatives on cascade hole injection. When an additional TCTA layer was added, the EL spectra showed only the emission from FIr6. Both the external quantum efficiency and brightness significantly improved compared with those of the device using PEDOT/PSS as HTL (Table 2). When the cross-linked TCTA-BVB was used as the second HTL, the efficiency reached 3.17% at the brightness of 441 cd/m^2. The maximum brightness also increased to 17 400 cd/m^2 at 9.5 V. The improvement of both light output and quantum efficiency demonstrates that the utilization of double HTLs with better-matched HOMO levels improves the efficient hole injection from ITO to EML and facilitates more balanced charge transport. Although Bu-TCTA-PFCB forms slightly smoother films than TCTA-PFCB, the device using Bu-TCTA-PFCB as HTL shows much higher turn-on and driving voltages compared with those obtained from either TCTA-PFCB or cross-linked TCTA-BVB. It may be due to the insulating butyl groups that inhibit hole transport in the devices (Figure 8).

The compatibility between two different HTLs also significantly affects the device characteristics and reproducibility. Because of the significant dewetting of the cross-linked TFV-containing TCTAs on top of PS-TPD-PFCB, the devices made from these HTLs break down quite easily and have very poor reproducibility. On the contrary, the devices made from cross-linked TCTA-BVB and PS-TPD-PFCB HTLs can be repeatedly biased to their maximum luminance because of their morphological stability.

Conclusions

A series of TCTA derivatives that are functionalized with thermally cross-linkable trifluorovinyl ether groups (TCTA-TTFV, Bu-TCTA-TTFV) or vinylbenzyl ether groups (TCTA-BVB) have been synthesized to explore their use as efficient hole-injecting and hole-transporting materials. Their excellent solvent resistance allows them to be used for cascade hole injection in blue-emitting electrophosphorescent devices. The effects of cross-linking temperature and functional groups on the compatibility between two HTLs are investigated through optical and atomic force microscopy. The vinylbenzyl-ether-containing TCTA provides the best compatibility with the bottom HTL. The resulting light-emitting device reaches a peak external quantum efficiency of 3.17%, corresponding to a current efficiency of 6.6 cd/A; these values are 2 times higher than those of PLEDs that use the conventional PEDOT/PSS as a single HTL. The improvements in the device performance are due to reduced hole-injection barrier and better electron/exciton confinement.

References and Notes

(1) Friend, R. H.; Gymer, R. W.; Burroughes, J. H.; Marks, R. N.; Taliani, C.; Bradley, D. D. C.; dos Santos, D. A.; Brédas, J. L.; Lögdlund, M.; Salaneck, W. *Nature* **1999**, *397*, 121.
(2) Parker, D.; Pei, Q.; Marrocco, M. *Appl. Phys. Lett.* **1994**, *65*, 1272.
(3) Gruener, J. H.; Wittmann, F.; Hamer, P. J.; Friend, R. H.; Huber, J.; Scherf, U.; Muellen, K.; Moratti, S. C.; Holmes, A. B. *Synth. Met.* **1994**, *67*, 181.
(4) Braig, T.; Müller, D. C.; Gross, M.; Meerholz, K.; Nuyken, O. *Macromol. Rapid Commun.* **2000**, *21*, 583.
(5) Zhang, Y.-D.; Hreha, R. D.; Jabbour, G. E.; Kippelen, B.; Peyghambarian, N.; Marder, S. R. *J. Mater. Chem.* **2002**, *12*, 1703.
(6) Bayerl, M. S.; Braig, T.; Nuyken, O.; Müller, D. C.; Gross, M.; Meerholz, K. *Macromol. Rapid Commun.* **1999**, *20*, 224.
(7) Liu, S.; Jiang, X.; Ma, H.; Liu, M. S.; Jen, A. K.-Y. *Macromolecules* **2000**, *33*, 3514.
(8) Jiang, X.; Liu, S.; Liu, M. S.; Hergurth, P.; Jen, A. K.-Y.; Fong, H.; Sarikaya, M. *Adv. Funct. Mater.* **2002**, *12*, 745.
(9) Bozano, L. D.; Carter, K. R.; Lee, V. Y.; Miller, R. D.; DiPietro, R.; Scott, J. C. *J. Appl. Phys.* **2003**, *94*, 3061.
(10) Chou, M.-Y.; Leung, M.-K.; Su, Y. O.; Chiang, C. L.; Lin, C.-C.; Liu, J.-H.; Kuo, C.-K.; Mou, C.-Y. *Chem. Mater.* **2004**, *16*, 654.
(11) Suzuki, M.; Tokito, S.; Sato, F.; Igarashi, T.; Kondo, K.; Koyama, T.; Yamaguchi, T. *Appl. Phys. Lett.* **2005**, *86*, 103507.
(12) Vaeth, K. M.; Tang, C. W. *J. Appl. Phys.* **2002**, *92*, 3447.
(13) Jiang, C.; Yang, W.; Peng, J.; Xiao, S.; Cao, Y. *Adv. Mater.* **2004**, *16*, 537.
(14) Gong, X.; Ostrowski, J. C.; Bazan, G. C.; Moses, D.; Heeger, A. J.; Liu, M. S.; Jen, A. K.-Y. *Adv. Mater.* **2003**, *15*, 45.
(15) Niu, Y.-H.; Tung, Y.-L.; Chi, Y.; Shu, C.-F.; Kim, J.-H.; Chen, B.; Luo, J.; Carty, A. J.; Jen, A. K.-Y. *Chem. Mater.* **2005**, *17*, 3532.
(16) Chen, F.-C.; Chang, S.-C.; He, G.; Pyo, S.; Yang, Y.; Kurotaki, M.; Kido, J. *J. Polym. Sci., Part B: Polym. Phys.* **2003**, *41*, 2681.
(17) Sudhakar, M.; Djurovich, P. I.; Hogen-Esch, T. E.; Thompson, M. E. *J. Am. Chem. Soc.* **2003**, *125*, 7796.

(18) Kuwabara, Y.; Ogawa, H.; Inada, H.; Noma, N.; Shirota, Y. *Adv. Mater.* **1994**, *6*, 677.
(19) Wu, C.-C.; Lin, Y.-T.; Wong, K.-T.; Chen, R.-T.; Chie, Y.-Y. *Adv. Mater.* **2004**, *1*, 6–61.
(20) Ren, X.; Li, J.; Holmes, R. J.; Djurovich, P. I.; Forrest, S. R.; Thompson, M. E. *Chem. Mater.* **2004**, *16*, 4743.
(21) Müller, D. C.; Braig, T.; Nothofer, H.-G.; Arnoldi, M.; Gross, M.; Scherf, U.; Nuyken, O.; Meerholz, K. *Chem. Phys. Chem.* **2000**, *4*, 207.
(22) Morgado, J.; Friend, R. H.; Cacialli, F. *Appl. Phys. Lett.* **2002**, *80*, 2436.
(23) Ego, C.; Grimsdale, A. C.; Uckert, F.; Yu, G.; Srdanov, G.; Mullen, K. *Adv. Mater.* **2002**, *14*, 809.
(24) Kim, J.-S.; Friend, R.; Grizzi, I.; Burroughes, J. H. *Appl. Phys. Lett.* **2005**, *87*, 023506-1.
(25) Choulis, S. A.; Choong, V.-E.; Mathai, M. K.; So, F. *Appl. Phys. Lett.* **2005**, *87*, 113503–1.
(26) Gong, X.; Wang, S.; Moses, D.; Bazan, G. C.; Heeger, A. J. *Adv. Mater.* **2005**, *17*, 2053.
(27) Yan, H.; Lee, P.; Armstrong, N. R.; Graham, A.; Evmenenko, G. A.; Dutta, P.; Marks, T. J. *J. Am. Chem. Soc.* **2005**, *127*, 3172.
(28) Liu, S.; Jen, A. K.-Y. Unpublished result.
(29) Holmes, R. J.; D'Andrade, B. W.; Forrest, S. R.; Ren, X.; Li, J.; Thompson, M. E. *Appl. Phys. Lett.* **2003**, *83*, 3818.
(30) Hamaguchi, M.; Yoshino, K. *Jpn. J. Appl. Phys.* **1996**, *35*, 4813.
(31) D'Andrade, B. W.; Holmes, R. J.; Forrest, S. R. *Adv. Mater.* **2004**, *16*, 624.
(32) Marsal, P.; Avilov, I.; da Silva Filho, D. A.; Bredas, J. L.; Beljonne, D. *Chem. Phys. Lett.* **2004**, *392*, 521.
(33) Li, J.; Djurovich, P. I.; Alleyne, B. D.; Tsyba, I.; Ho, N. N.; Bau, R.; Thompson, M. E. *Polyhedron.* **2004**, *23*, 419.
(34) Shi, J.; Tang, C. W.; Chen, C. H. U.S. Patent 5645948, **1997**.
(35) Chen, J. P. WO Patent **059014, 2003**.
(36) Shirota, Y. *J. Mater. Chem.* **2000**, *10*, 1.
(37) Katrizky, A. R.; Wang, Z. *J. Heterocycl. Chem.* **1988**, *25*, 671.
(38) Ligon, S. C. J.; Topping, C. M.; Jin, J.; Fallis, S.; Irvin, J. A.; Desmarteau, D. D.; Smith, D. W. J. *Macromol. Chem. Phys.* **2004**, *205*, 801.
(39) Spraul, B.; Suresh, S.; Glaser, S.; Perahia, D.; Ballato, J.; Smith, D. W. J. *J. Am. Chem. Soc.* **2004**, *126*, 12772.
(40) Kläner, G.; Lee, J.-I.; Lee, V. Y.; Chan, E.; Chen, J.-P.; Nelson, C. A.; Markiewicz, D.; Siemens, R.; Scott, J. C.; Miller, R. D. *Chem. Mater.* **1999**, *11*, 1800.

MA801374W